Editors' Suggestion

Anomalous Aharonov-Bohm Interference in the Presence of Edge Reconstruction

Sourav Biswas, Hemanta Kumar Kundu, Rajarshi Bhattacharyya, Vladimir Umansky, and Moty Heiblum*
Braun Center for Submicron Research, Department of Condensed Matter Physics, Weizmann Institute of Science, Rehovot 7610001, Israel

(Received 11 June 2023; revised 18 September 2023; accepted 19 January 2024; published 12 February 2024)

Interferometry is a vital tool for studying fundamental features in the quantum Hall effect. For instance, Aharonov-Bohm interference in a quantum Hall interferometer can probe the wave-particle duality of electrons and quasiparticles. Here, we report an unusual Aharonov-Bohm interference of the outermost edge mode in a quantum Hall Fabry-Pérot interferometer, whose Coulomb interactions were suppressed with a grounded drain in the interior bulk of the interferometer. In a descending bulk filling factor from $\nu_{\mathbf{b}} = 3$ to $\nu_{\mathbf{b}} \approx (5/3)$, the magnetic field periodicity, which corresponded to a single "flux quantum," agreed accurately with the enclosed area of the interferometer. However, in the filling range, $\nu_{\mathbf{b}} \approx (5/3)$ to $\nu_{\mathbf{b}} = 1$, the field periodicity increased markedly, *a priori* suggesting a drastic shrinkage of the Aharonov-Bohm area. Moreover, the modulation gate voltage periodicity decreased abruptly at this range. We attribute these unexpected observations to edge reconstruction, leading to area changing with the field and a modified modulation gate-edge capacitance. These reproducible results support future interference experiments with a quantum Hall Fabry-Pérot interferometer.

DOI: 10.1103/PhysRevLett.132.076301

A two-dimensional electron gas (2DEG), subjected to a strong perpendicular magnetic field, exhibits quantized plateaus of the electrical Hall conductance, $\sigma_{xy} = \nu(e^2/h)$, where e is the electron charge, h is the Planck constant, and v is the filling factor (integer or fraction). In a quantum Hall (QH) system, gapless, chiral, 1D-like edge modes carry the current while the bulk is insulating [1–5]. Carriers can be electrons or fractionally charged quasiparticles [6–8], with the latter obeying anyonic exchange statistics, with the quasiparticle exchange phase π/m at a filling $\nu = 1/m$ [9–17]. Studying the edge modes allows for discerning the properties of the bulk (due to "bulk-edge correspondence"). Examples are the studies of shot noise [18], thermal transport [19], and interference [20].

Interferometry with QH edge modes provides an excellent tool for investigating the wave nature of electrons and quasiparticles, their coherence, and statistics. The customarily employed interferometers in the QH regime are the multipath Fabry-Pérot interferometer (FPI) [13,21–30] and the two-path Mach-Zehnder interferometer (MZI) [14,31–35]. While the MZI has a built-in metallic drain, thus operating in the Aharonov-Bohm (AB) regime, an unscreened FPI is affected by Coulomb interactions [36,37], which tend to mask the AB interference. Screening these interactions with parallel conducting layers [13,27], a metallic top gate [21,22], or via draining charges by an internal grounded drain [23,25] reveal AB interference. Anyonic statistics had been recently observed in a screened FPI [13].

Here, we studied interference in FPIs with an internal grounded drain in the bulk filling factor ranging from $\nu_b = 3$ to $\nu_b = 1$. As detailed below, an anomalous interference of the outermost integer edge mode appears concomitantly with the emergence of edge reconstruction at $\nu_b \approx 5/3$ [38–40].

A ubiquitous FPI consists of two partitioning quantum point contacts (QPCs) serving as beam splitters, a gated (or etched) confined bulk, and a "modulation gate" (Supplemental Material, Fig. S1 [41]). The latter depletes the bulk locally, thus changing the area enclosed by the interfering edge mode, $\delta A = \alpha \delta V_{MG}$, with α a function of the gate-edge capacitance and the carrier density. The AB flux periodicity of the interfering integer edge mode is the flux quantum, $\Phi_0 = h/e$, with a winding phase $\varphi_{AB} = 2\pi BA/\Phi_0$, where A is the enclosed area and B the magnetic field [42]. For weakly backscattering QPCs, the transmission probability is given by $T_{FPI} = |\tau|^2 = t_l^2 t_r^2 (1 + r_l^2 r_r^2 \cos_{AB})$, where $t_l^2(t_r^2)$ and $r_l^2(r_r^2)$ are the transmission and reflection probabilities of the left (right) QPC, respectively. In the fractional regime, the AB phase is modified, $\varphi_{AB} = (e^*/e)2\pi BA/\Phi_0$, leading to periodicities: $\Delta B = (e/e^*)\Phi_0/A$ and $\Delta A = (e/e^*)\Phi_0/B$.

The FPIs were fabricated in a high-mobility 2DEG embedded in GaAs-AlGaAs heterostructure at a depth of ~100 nm below the surface, with two different electron densities $(1.7\ \&\ 1.1) \times 10^{11}\ \mathrm{cm}^{-2}$ and an enclosed area between 5 μm^2 and 17 μm^2 (Fig. 1(a) and Supplemental Material, Fig. S2 [41]). The internal grounded drain dimensions varied between $450 \times 450\ \mathrm{nm}^2$ and $800 \times 800\ \mathrm{nm}^2$, respectively. Differential conductance was measured by applying a small ac voltage of 1 μV_{RMS} at 900 KHz at 10 mK. The signal was amplified by a cooled preamplifier (at 1.5 K) cascaded by a room-temperature amplifier.

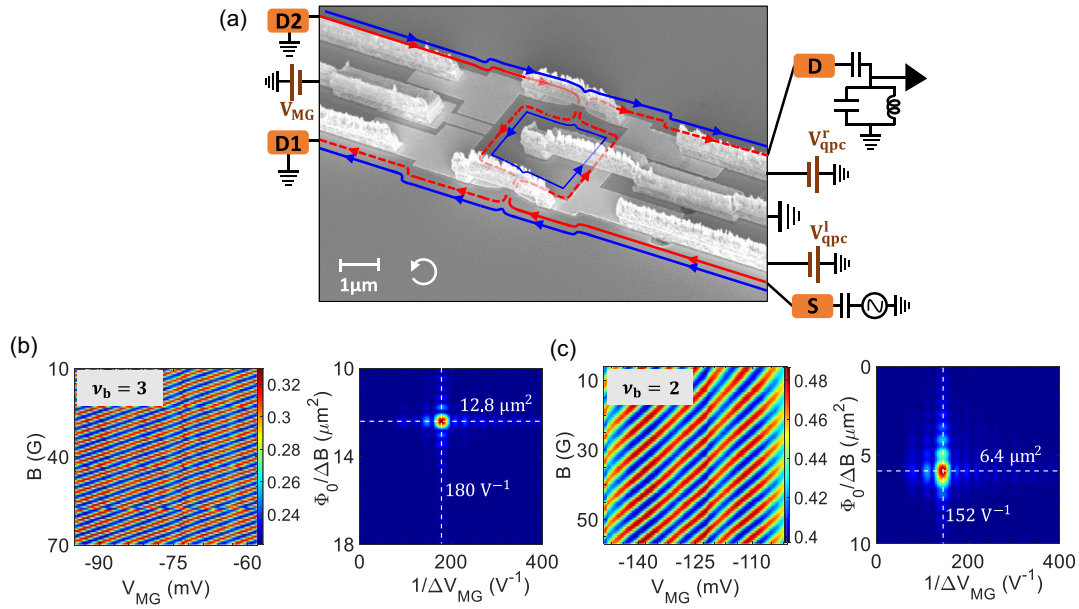

FIG. 1. Device structure and Aharonov-Bohm oscillations at $\nu_b = 3, 2$. (a) Scanning electron micrograph image of a Fabry-Pérot interferometer with a grounded drain at the center bulk. Standard ohmic contacts of alloyed Ni-Au-Ge served as source (S) and drain (D), and thin metallic PdAu-Au served as gates. The split gates as QPCs were 450 nm apart, and the modulation gate was 300 nm wider. The lithographic internal area of the device is 10.25 μm^2. Red and blue lines represent the outermost and the inner edge modes, respectively. The dashed lines show reflected and transmitted edge modes. The inner edge mode is fully reflected. (b),(c) Typical Aharonov-Bohm pajama in $B - V_{MG}$ plane at filling factor $\nu_b = 3 (B = 2.33$ T) and $\nu_b = 2 (B = 3.6$ T), when the integer outer edge $\nu_e = 1$ is weakly partitioned with the transmission probability $t_{l,r}{}^2 \approx 0.93$. Respective fast Fourier transformation with the unique frequencies in B and V_{MG} are shown on the right. The values of ΔB and ΔV_{MG} follow the usual AB interference equation resulting in the flux periodicity of Φ_0 at $\nu_b = 2$, and $\Phi_0/2$ at $\nu_b = 3$.

We start with interfering the outermost integer edge mode, $\nu_e = 1$ at fillings $\nu_b = 3$ and $\nu_b = 2$ in an FPI with an area of $\sim$10.25 μm^2 fabricated in higher density (1.7×10^{11} cm^{-2}) 2DEG. The conductance plot in the $B - V_{MG}$ plane [42] has the familiar AB-type *pajama* pattern [Figs. 1(b) and 1(c)], clearly proving a typical AB interference. The AB periodicities at $\nu_b = 2$ are $\Delta B = 6.4$ G and $\Delta V_{MG} = 6.58$ mV, corresponding to electron interference with a flux periodicity of Φ_0. However, at $\nu_b = 3$ we find $\Delta B = 3.2$ G and $\Delta V_{MG} = 5.55$ mV corresponding to a flux periodicity of $\Phi_0/2$ being the known (but not fully understood) pairing phenomenon of the interfering electrons with $e^* \approx 2e$ [23,43,44]. Throughout the filling range $\nu_b = [3, 5/3]$, the corresponding AB area is $A = (e/e^*)(\Phi_0/\Delta B) = 6.4$ μm^2, suggesting gate-induced lateral depletion of some ≈350 nm.

At the filling factor $\nu_b \approx 5/3$, a dramatic change in the interference pattern takes place. Monitoring the interference of $\nu_e = 1$ in a progressively declining filling factor between $\nu_b \approx 5/3$ and $\nu_b = 1$, the field periodicity increases from $\Delta B = 6.4$ G to $\Delta B = 18.6$ G, respectively; see Figs. 2(a) and 2(b) and the Supplemental Material, Fig. S4 [41], for the AB pajama at $\nu_b = 1$. Also, the modulation gate voltage periodicity decreases unexpectedly with lower filling in the same filling range. Note that during interference of the outer edge mode, the inner edge mode is fully reflected by the first QPC, i.e., the filling at the QPC is always below 1.

The dramatic change in the field periodicity in the range $\nu_b = [5/3, 1]$ suggests *a priori* a monotonic shrinkage of the area $(\Phi_0/\Delta B)$—by a factor of around 3 at $\nu_b = 1$ (Fig. 3(a) and Supplemental Material, Fig. S5 [41]). However, since FPIs with different lithographic areas exhibit similar behavior, i.e., an approximately similar factor of increase in ΔB, see Fig. 3(a), such apparent "area change" cannot occur. What is so unique in $\nu_b \approx 5/3$ and lower filling that leads to such abnormal behavior?

We recently found an emergent edge reconstruction of the outermost edge mode starting at $\nu_b \approx 5/3$ and persisting until at least $\nu_b = 1$, while for $\nu_b > 5/3$, edge reconstruction was not observed [38]. Below $\nu_b \approx 5/3$, the outer integer filling $\nu_e = 1$ was reconstructed to two fractional states: an outermost $\nu_e = 1/3$ and an inner $\nu_e = 2/3$ [38,45,46], with a $e^2/3h$ conductance plateau observed in the transmission of a QPC [Fig. 2(c)]. Beyond an equilibration distance, an upstream bosonic neutral mode is born [Fig. 2(d)]. Approaching $\nu_b = 1$, edge reconstruction and the excitation of the neutral mode strengthen. Based on these observations, we propose a mechanism explaining the anomalous behavior of the FPI.

The enclosed flux evolution is $\Delta\Phi = \Delta B * A - B * \Delta A$, with A as the enclosed area. Assume that with increasing B the enclosed area does not remain constant, leading to $(1/A)(\Delta\Phi/\Delta B) = 1 - (B/\Delta B)(\Delta A/A)$. For filling

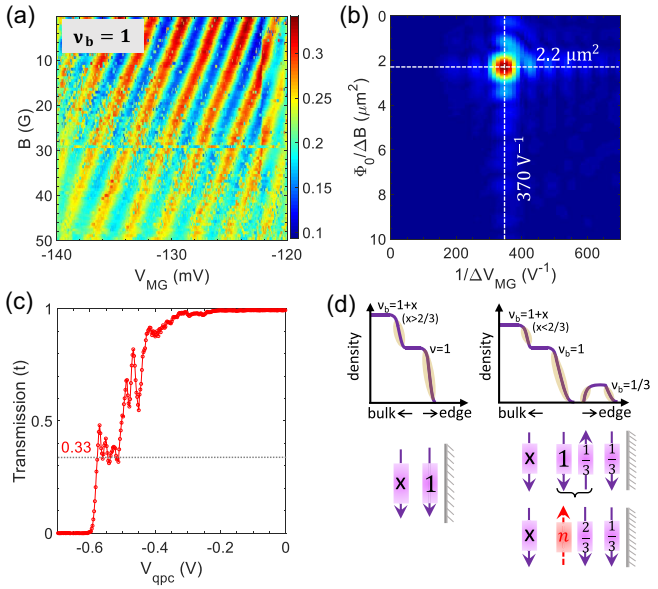

FIG. 2. Aharonov-Bohm interference and the reconstructed edge at $\nu_b = 1$ measured with the interferometer with an area 10.25 μm^2 and the higher electron density. (a) The characteristic pajama with the Aharonov-Bohm (AB) slope at the filling factor $\nu_b = 1 (B = 6.4$ T). The QPCs' transmissions are $t_{l,r}{}^2 \approx 0.46$. (b) The fast Fourier transformation shows a single peak with periodicity, $\Delta V_{MG} = 2.7$ mV and $\Delta B = 18.6$ G, drastically different from what is expected from $\nu_b = 2$. Comparing the periodicities at $\nu_b = 2$ and $\nu_b = 1$, the latter suggests an AB flux periodicity of $2.9\Phi_0$ (in B-dependence) but $0.73\Phi_0$ (in V_{MG}-dependence)—hence unacceptable. (c) The conductance as the QPC transmission measured at $B = 6.4$ T shows a plateau of 1/3 due to edge reconstruction. Interference is measured at different transmission values with the QPCs weakly and strongly pinched (see Supplemental Material, Fig. S4 [41]). (d) Schematic representation of the density profile below and above the bulk filling $\nu_b = 5/3$, and the reconstruction of the outer edge mode $\nu_e = 1$. The edge modes are shown below by the purple arrow. Below $\nu_b = 5/3$, the creation of 1/3 density near the edge leads to two counterpropagating 1/3 modes. The modes' equilibration leads to two downstream 2/3 and 1/3 modes, and an upstream neutral mode (red dashed arrow) such that the net thermal Hall conductance κ_{xy} remains conserved.

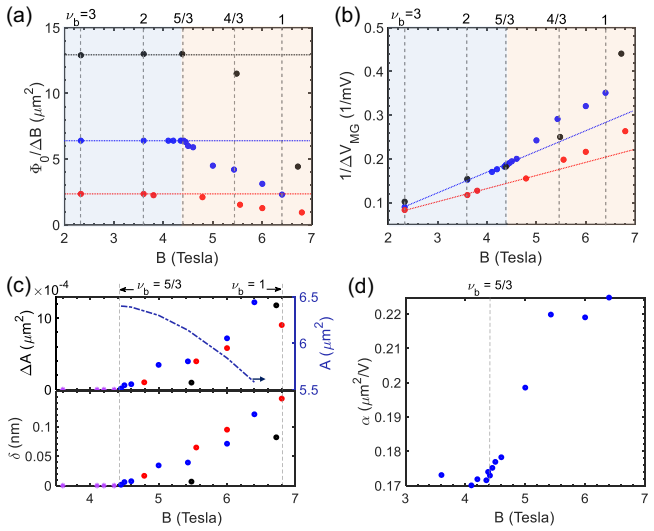

FIG. 3. Anomalous periodicity of interference at $\nu_b < 5/3$. (a), (b) Variation of field- and modulation gate-periodicities with filling factors ranging from $\nu_b = 3$ to 1 for three different devices of lithographic internal area 17.2 μm^2 (black), 10.25 μm^2 (blue), and 4.87 μm^2 (red). The estimated apparent area $(\Phi_0/\Delta B)$ as a function of the magnetic field (B) shows a monotonic decrease below the filling $\nu_b \approx 5/3$. Similarly, the frequency $(1/\Delta V_{MG})$ with B also diverts from the usual linear slope of electrons' interference below $\nu_b \approx 5/3$. In the Supplemental Material, Fig. S5 [41], a few pajamas with the fast Fourier transformation around the filling of 5/3 for a device are shown. (c) The calculated change in area ΔA, the (effective) area A, and the amount of inward shift δ of the edge mode using the measured ΔB and the flux evolution equation. For $\nu_b > 5/3$, $\Delta A = 0$ and $\delta = 0$ (shown by purple stars). In the range $\nu_b = 5/3$ to 1, ΔA and δ increase with B (shown by solid circles). The blue dashed line (top figure) with the right y axis shows the actual Aharonov-Bohm area (for a device represented in blue) in the range $\nu_b = 5/3$ to 1 after incorporating the effect of ΔA. Note that the area shrinks by ~1 μm^2, i.e., approximately 1.1 times contrary to the *a priori* area shrinking by 3 times. (d) The mutual capacitance α, obtained from ΔV_{MG} values, for a device represented in blue dots showing its unusual variation below $\nu_b \approx 5/3$.

$\nu > 5/3$, where ΔB is constant, namely, $A * \Delta B = \Phi_0$ and $(1/A)(\Delta\Phi/\Delta B) = 1$, with $\Delta A = 0$—as expected. However, for $\nu < 5/3$, since the periodicity of ΔB increases monotonically with B, a finite reduction in the area, ΔA, must occur in each period of one flux quantum. The estimated magnitude of ΔA and A, with the measured values of B and ΔB, is shown in Fig. 3(c). The detailed method of calculating ΔA and for the addition of a flux quantum is described in the Supplemental Material, Sec. I [41]. Since $(B/\Delta B) \sim 10^4$, the relative change in the area is tiny,$(\Delta A/A) \sim 10^{-4}$, resulting from an inward shift δ of the circulating edge mode, $\delta = (\Delta A/4\sqrt{A})$, which is of the order of ~0.1 nm [Fig. 3(c)]. An alternative estimate of δ results in a nearly similar value to the above (Supplemental Material, Sec. II [41]). It is remarkable how a minute change in δ strongly affects the AB interference periodicity.

Being a crucial point, we stress it again. When the edge mode location becomes sensitive to the magnetic field, a significant contribution to the flux comes from the term $B * \Delta A$, being on the order of $A * \Delta B$. This appears erroneously as a large reduction in the area that is calculated solely via the term $A * \Delta B$ (see Fig. 3(c) and the Supplemental Material, Fig. S9 [41]).

At filling $\nu_b \approx 5/3$, due to edge reconstruction an incompressible strip is formed around the outermost edge, with fillings $\nu = 1/3$ and $\nu = 2/3$ [23]. With increasing the field (with further lower filling), this strip continues to widen, and thus in field scanning, the progressive change in area (ΔA) plays a significant role. Approaching $\nu_b = 1$, the increasing reconstruction strength and wider strip lead to

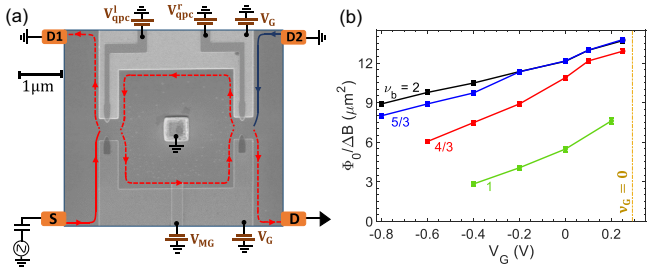

FIG. 4. Interferometer with variable edge potential and the magnetic field periodicity. (a) Scanning electron micrograph image of a fully gated Aharonov-Bohm (FPI) with the internal lithographic area of 14.2 μm^2, fabricated in the lower density (1.1×10^{11} cm^{-2}) 2DEG. The split gates (QPCs) are separated from the rest of the confining gates. Hafnium oxide separates the ohmic contacts (shown in yellow) from the gates and between the successive gate layers. The gate voltage V_G tunes the depletion and thus the edge potential. The QPC gate voltages V_{qpc} independently induce backscattering to the edge mode. (b) Obtained apparent area ($\Phi_0/\Delta B$) from the magnetic field periodicities at different depletion strengths of the FPI at various filling factors. More details of interference traces and 3D pajamas are shown in the Supplemental Material, Figs. S6 and S7 [41]. The confining gates' voltage, $V_G = 0.27$ V, is the value at which the filling under the gates is zero, $\nu_G = 0$ (shown by the dashed yellow line). With a more negative V_G, the active interior area shrinks significantly (e.g., ~36% reduces for $V_G = -0.8$ V at $\nu_b = 2$). Along any vertical cut (constant V_G line), crossing the filling $\nu_b \approx 5/3$, the anomaly in the value of $\Phi_0/\Delta B$ becomes apparent.

the proportional increase in δ with B. The higher (lower) δ for a smaller (larger) size device is consistent with the larger (smaller) ΔB, i.e., one needs to scan a longer (shorter) range of B for one flux quantum resulting in the wider (narrower) reconstructed strip.

Similarly, the dependence of $1/\Delta V_{MG}$ on B, with ΔV_{MG} the voltage required to change the AB flux by one flux quantum changes abruptly at $\nu_b \approx 5/3$ (with $\Delta\Phi = B * \Delta A$) [Fig. 3(b)]. The incremental depleted charge, $\Delta Q = ne\Delta A = C_{MG}\Delta V_{MG}$, or equivalently $(1/\Delta V_{MG}) = (C_{MG}/ne) * (B/\Phi_0)$, where n is the charge density, C_{MG} is the gate-edge capacitance, and $\alpha = (C_{MG}/ne)$. Using the measured ΔV_{MG}, α is plotted as a function of B in Fig. 3(d). While α is nearly constant (as expected) for $\nu_b > 5/3$, it increases at fillings $\nu_b < 5/3$. The larger α is a result of the lower charge density in the reconstructed lower filling (e.g., $\nu = 1/3$) region. The latter getting stronger leads to the continuous increase in α with B.

Since edge reconstruction can depend on the sharpness of the edge potential, we repeated these measurements in an FPI, which allows tunable pinching [Fig. 4(a)]. We tested the frequency $\Phi_0/\Delta B$ with a more substantial confining potential (via V_G) in the range $\nu_b = 3$ to $\nu_b = 1$ [Fig. 4(b)]. We find the following: (*i*) the AB area decreases drastically with increasing gate depletion, and (*ii*) the anomaly in the periodicity for fillings $\nu_b < 5/3$ persists and suggests that edge reconstruction and neutral modes cannot be fully quenched. In the Supplemental Material, Fig. S8 [41], we describe similar experiments performed in an MZI, where there is nearly no change in the AB area. Indeed, the two interfering trajectories in an MZI shift in the same direction with B, while in the FPI the trajectories move in the opposite direction [47].

The FPI is the simplest and thus frequently employed in the quantum Hall regime. When a ubiquitous edge reconstruction occurs, topological or trivial, the AB electron interference becomes anomalous. In contrast to the expected periodicities in the magnetic field and gate voltage, a gradual increase in the periodicity is observed with an increasing magnetic field, accompanied by an abnormal decrease in the gate voltage periodicity. Our results, revealing a new effect on AB interference, suggest that the details of edge structure—often not considered—may be critical in interpreting the AB-FPI interference oscillations. For instance, in the earlier FPI experiments with fractional states, the weaker magnetic field dependent oscillations may indicate the AB flux periodicity of Φ_0 with a modified area due to edge mode position at that filling factor. The area must be ensured correctly in future FPI studies.

We thank Mitali Banerjee, Dima E. Feldman, Yuval Gefen, Bertrand I. Halperin, Bernd Rosenow, and Ady Stern for useful discussions. S. B. acknowledges Abhay Kumar Nayak for his technical help. We acknowledge the continuous support of the Sub-Micron Center staff. M. H. acknowledges the support of the European Research Council under the European Union's Horizon 2020 research and innovation program (Grant Agreement No. 833078) and the partial support of the Minerva Foundation with funding from the Federal German Ministry for Education and Research, under Grant No. 713534. S. B., R. B., and H. K. K. fabricated the devices and performed the measurements. S. B., H. K. K., and M. H. analyzed the data, discussed the results, and wrote the paper. V. U. grew the GaAs heterostructures. M. H. supervised the experiments.

*Corresponding author: moty.heiblum@weizmann.ac.il

[1] R. Prange and S. M. Girvin, *The Quantum Hall Effect* (Springer Verlag, Berlin, 1990).
[2] S. D. Sarma and A. Pinczuk, *Perspective in Quantum Hall Effects* (Wiley, New York, 1996).
[3] B. I. Halperin and J. K. Jain, *Fractional Quantum Hall Effects: New Developments* (World Scientific, Singapore, 2020).
[4] B. I. Halperin, Quantized Hall conductance, current-carrying edge states, and the existence of extended states in a two-dimensional disordered potential, Phys. Rev. B **25**, 2185 (1982).

[5] C. L. Kane and M. P. A. Fisher, in *Perspectives in Quantum Hall Effects: Novel Quantum Liquids in Low-Dimensional Semiconductor Structures*, edited by S. Das Sarma and A. Pinczuk (John Wiley, New York, 1996).

[6] R. B. Laughlin, Anomalous quantum Hall effect: An incompressible quantum fluid with fractionally charged excitations, Phys. Rev. Lett. **50**, 1395 (1983).

[7] R. dePicciotto, M. Reznikov, M. Heiblum, V. Umansky, G. Bunin, and D. Mahalu, Direct observation of a fractional charge, Nature (London) **389**, 162 (1997).

[8] L. Saminadayar, D. C. Glattli, Y. Jin, and B. Etienne, Observation of the $e/3$ fractionally charged Laughlin quasiparticle, Phys. Rev. Lett. **79**, 2526 (1997).

[9] F. D. Haldane, "Fractional statistics" in arbitrary dimensions: A generalization of the Pauli principle, Phys. Rev. Lett. **67**, 937 (1991).

[10] A. Stern, Anyons and the quantum Hall effect—A pedagogical review, Ann. Phys. (Amsterdam) **323**, 204 (2008).

[11] D. E. Feldman and B. I. Halperin, Fractional charge and fractional statistics in the quantum Hall effects, Rep. Prog. Phys. **84**, 076501 (2022).

[12] H. Bartolomei *et al.*, Fractional statistics in anyon collisions, Science **368**, 173 (2020).

[13] J. Nakamura, S. Liang, G. C. Gardner, and M. J. Manfra, Direct observation of anyonic braiding statistics, Nat. Phys. **16**, 931 (2020).

[14] H. K. Kundu, S. Biswas, N. Ofek, V. Y. Umansky, and M. Heiblum, Anyonic interference and braiding phase in a Mach-Zehnder interferometer, Nat. Phys. **19**, 515 (2023).

[15] J.-Y. M. Lee, C. Hong, T. Alkalay, N. Schiller, V. Umansky, M. Heiblum, Y. Oreg, and H.-S. Sim, Partitioning of diluted anyons reveals their braiding statistics, Nature (London) **617**, 277 (2023).

[16] P. Glidic, O. Maillet, A. Aassime, C. Piquard, A. Cavanna, U. Gennser, Y. Jin, A. Anthore, and F. Pierre, Cross-correlation investigation of anyon statistics in the $\nu = 1/3$ and $2/5$ fractional quantum Hall states, Phys. Rev. X **13**, 011030 (2023).

[17] M. Ruelle, E. Frigerio, J. M. Berroir, B. Plaçais, J. Rech, A. Cavanna, U. Gennser, Y. Jin, and G. Fève, Comparing fractional quantum Hall Laughlin and Jain topological orders with the anyon collider, Phys. Rev. X **13**, 011031 (2023).

[18] M. Heiblum, Quantum shot noise in edge channels, Phys. Status Solidi B **243**, 3604 (2006).

[19] C. L. Kane and M. P. A. Fischer, Quantized thermal transport in the fractional quantum Hall effect, Phys. Rev. B **55**, 15832 (1997).

[20] M. Carrega, L. Chirolli, S. Heun, and L. Sorba, Anyons in quantum Hall interferometry, Nat. Rev. Phys. **3**, 698 (2022).

[21] Y. M. Zhang, D. T. McClure, E. M. Levenson-Falk, C. M. Marcus, L. N. Pfeiffer, and K. W. West, Distinct signatures for Coulomb blockade and Aharonov-Bohm interference in electronic Fabry-Perot interferometers, Phys. Rev. B **79**, 241304(R) (2009).

[22] N. Ofek, A. Bid, M. Heiblum, A. Stern, V. Umansky, and D. Mahalu, Role of interactions in an electronic Fabry–Perot interferometer operating in the quantum Hall effect regime, Proc. Natl. Acad. Sci. U.S.A. **107**, 5276 (2010).

[23] H. K. Choi, I. Sivan, A. Rosenblatt, M. Heiblum, V. Umansky, and D. Mahalu, Robust electron pairing in the integer quantum Hall effect regime, Nat. Commun. **6**, 7435 (2015).

[24] I. Sivan, H. K. Choi, J. Park, A. Rosenblatt, Y. Gefen, D. Mahalu, and V. Umansky, Observation of interaction-induced modulations of a quantum Hall liquid's area, Nat. Commun. **7**, 12184 (2016).

[25] I. Sivan, R. Bhattacharyya, H. K. Choi, M. Heiblum, D. E. Feldman, D. Mahalu, and V. Umansky, Interaction-induced interference in the integer quantum Hall effect, Phys. Rev. B **97**, 125405 (2018).

[26] D. T. McClure, W. Chang, C. M. Marcus, L. N. Pfeiffer, and K. W. West, Fabry-Perot interferometry with fractional charges, Phys. Rev. Lett. **108**, 256804 (2012).

[27] J. Nakamura, S. Fallahi, H. Sahasrabudhe, R. Rahman, S. Liang, G. C. Gardner, and M. J. Manfra, Aharonov–Bohm interference of fractional quantum Hall edge modes, Nat. Phys. **15**, 563 (2019).

[28] R. L. Willett, L. N. Pfeiffer, and K. W. West, Measurement of filling factor $5/2$ quasiparticle interference with observation of charge $e/4$ and $e/2$ period oscillations, Proc. Natl. Acad. Sci. U.S.A. **106**, 8853 (2009).

[29] Y. Ronen *et al.*, Aharonov–Bohm effect in graphene-based Fabry–Pérot quantum Hall interferometers, Nat. Nanotechnol. **16**, 563 (2021).

[30] C. Déprez, L. Veyrat, H. Vignaud, G. Nayak, K. Watanabe, T. Taniguchi, F. Gay, H. Sellier, and B. Sacépé, A tunable Fabry–Pérot quantum Hall interferometer in graphene, Nat. Nanotechnol. **16**, 555 (2021).

[31] Y. Ji, Y. Chung, D. Sprinzak, M. Heiblum, D. Mahalu, and H. Shtrikman, An electronic Mach-Zehnder interferometer, Nature (London) **422**, 415 (2003).

[32] I. Neder, N. Ofek, Y. Chung, M. Heiblum, D. Mahalu, and V. Umansky, Interference between two indistinguishable electrons from independent sources, Nature (London) **448**, 333 (2007).

[33] M. Jo *et al.*, Quantum Hall valley splitters and a tunable Mach-Zehnder interferometer in graphene, Phys. Rev. Lett. **126**, 146803 (2021).

[34] P. Roulleau, F. Portier, D. C. Glattli, P. Roche, A. Cavanna, G. Faini, U. Gennser, and D. Mailly, Finite bias visibility of the electronic Mach-Zehnder interferometer, Phys. Rev. B **76**, 161309(R) (2007).

[35] B. Karmakar, D. Venturelli, L. Chirolli, V. Giovannetti, R. Fazio, S. Roddaro, L. N. Pfeiffer, K. W. West, F. Taddei, and V. Pellegrini, Nanoscale Mach-Zehnder interferometer with spin-resolved quantum Hall edge states, Phys. Rev. B **92**, 195303 (2015).

[36] B. Rosenow and B. I. Halperin, Influence of interactions on flux and back-gate period of quantum Hall interferometers, Phys. Rev. Lett. **98**, 106801 (2007).

[37] S. N. Dinh and D. A. Bagrets, Influence of Coulomb interaction on the Aharonov-Bohm effect in an electronic Fabry-Pérot interferometer, Phys. Rev. B **85**, 073403 (2012).

[38] R. Bhattacharyya, M. Banerjee, M. Heiblum, D. Mahalu, and V. Umansky, Melting of interference in the fractional quantum Hall effect: Appearance of neutral modes, Phys. Rev. Lett. **122**, 246801 (2019).

[39] X. Wan, K. Yang, and E. H. Rezayi, Reconstruction of fractional quantum Hall edges, Phys. Rev. Lett. **88**, 056802 (2002).

[40] J. Wang, Y. Meir, and Y. Gefen, Edge reconstruction in the $\nu = 2/3$ fractional quantum Hall state, Phys. Rev. Lett. **111**, 246803 (2013).

[41] See Supplemental Material at http://link.aps.org/supplemental/10.1103/PhysRevLett.132.076301 for more images of the devices, additional data on the interference, and the detailed theoretical analysis.

[42] B. I. Halperin, A. Stern, I. Neder, and B. Rosenow, Theory of the Fabry-Perot quantum Hall interferometer, Phys. Rev. B **83**, 155440 (2011).

[43] S. Biswas, H. K. Kundu, V. Umansky, and M. Heiblum, Electron pairing of interfering interface-based edge modes, Phys. Rev. Lett. **131**, 096302 (2023).

[44] G. A. Frigeri and B. Rosenow, Electron pairing in the quantum Hall regime due to neutralon exchange, Phys. Rev. Res. **2**, 043396 (2020).

[45] U. Khanna, M. Goldstein, and Y. Gefen, Fractional edge reconstruction in integer quantum Hall phases, Phys. Rev. B **103**, L121302 (2021).

[46] S. Biswas, R. Bhattacharyya, H. K. Kundu, A. Das, M. Heiblum, V. Y. Umansky, M. Goldstein, and Y. Gefen, Shot noise does not always provide the quasiparticle charge, Nat. Phys. **18**, 1476 (2022).

[47] D. E. Feldman and B. I. Halperin, Robustness of quantum Hall interferometry, Phys. Rev. B **105**, 165310 (2022).